Hindawi Publishing Corporation
Advances in Materials Science and Engineering
Volume 2015, Article ID 952879, 11 pages
http://dx.doi.org/10.1155/2015/952879

Research Article

A Microstructural Study of Load Distribution in Cartilage: A Comparison of Stress Relaxation versus Creep Loading

Ashvin Thambyah,[1] V. M. van Heeswijk,[2] C. C. van Donkelaar,[2] and Neil Broom[1]

[1]*Experimental Tissue Mechanics Laboratory, Department of Chemical and Materials Engineering, University of Auckland, Auckland 1142, New Zealand*
[2]*Department of Biomedical Engineering, Eindhoven University of Technology, 5600 MB Eindhoven, Netherlands*

Correspondence should be addressed to Ashvin Thambyah; ashvin.thambyah@auckland.ac.nz

Received 24 February 2015; Accepted 19 May 2015

Academic Editor: Jun Liu

The compressive response of articular cartilage has been extensively investigated and most studies have focussed largely on the directly loaded matrix. However, especially in relation to the tissue microstructure, less is known about load distribution mechanisms operating outside the directly loaded region. We have addressed this issue by using channel indentation and DIC microscopy techniques that provide visualisation of the matrix microstructural response across the regions of both direct and nondirect loading. We hypothesise that, by comparing the microstructural response following stress relaxation and creep compression, new insights can be revealed concerning the complex mechanisms of load bearing. Our results indicate that, with stress relaxation, the initial mode of stress decay appears to primarily involve relaxation of the surface layer. In the creep loading protocol, the main mode of stress release is a lateral distribution of load via the mid matrix. While these two modes of stress redistribution have a complex relationship with the zonally differentiated tissue microstructure and the depth of strain, four *mechanostructural* mechanisms are proposed to describe succinctly the load responses observed.

1. Introduction

The response of articular cartilage to compressive loading may be described in terms of three primary force-related mechanisms: (1) the stresses that develop in the solid matrix, (2) the interstitial fluid pressure, and (3) the frictional drag that develops when fluid flows past the solid phase [1–3]. Dissipation of the frictional drag has been attributed to causing the overall viscoelastic response of cartilage [4, 5], following which the extent of the viscoelastic response is further determined by the rate of fluid exudation during compression [6]. The flow-independent intrinsic matrix viscoelasticity is an additional factor that contributes to the strain-rate dependency of cartilage [7, 8]. Besides viscoelastic effects of time and rate of loading, an additional complexity to the problem is that concerning the depth-dependent response of the cartilage matrix to compression. For example, with increasing compressive strain, stress relaxation proceeds at a reduced rate [9] and the average apparent modulus increases significantly [10]. Such a depth-dependent response has been attributed to the heterogeneity of cartilage structure and composition [11, 12] and thus presents additional considerations when studying cartilage mechanics.

Any accurate modelling of the mechanical behaviour of articular cartilage should thus ideally incorporate realistic structure and compositional effects, especially with regard to their depth-dependent variation. This clearly presents a major challenge as it involves transitioning across geometric scales of relatively macrolevel joint tissue loading and microlevel tissue structural response. For example, the actual depth-dependent microstructural response of the tissue could be determined and correlated with specific mechanical parameters derived from standard creep and stress relaxation tests. However, achieving any insight from such a correlation would depend on the extent to which matrix deformation can be visualised. Collagen fibrils are submicron in scale and form a complex interconnecting network which is "invisible" at the microlevel. Further, the fluid content within the matrix,

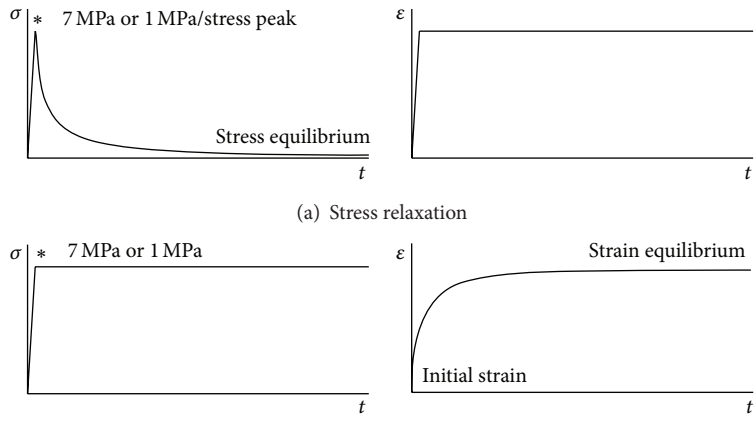

Figure 1: Schematic overview of the loading protocols used for stress relaxation and creep. Compression loading of either 7 MPa or 1 MPa was applied, indicated by the asterisks, followed by either (a) stress relaxation or (b) creep. For (a) stress relaxation, the position (strain) of the channel indenter was held constant while for (b) creep the load was held constant.

the hydrostatic stress build-up or displacement following direct loading of the matrix, has to be "visualised" in order to connect the macrolevel tissue mechanical properties with the microstructural response.

Recent studies have attempted to address these visualisation issues and two experimental procedures have been developed by the present researchers that have relevance to the question of how the cartilage matrix, with its *coupled* fluid phase, responds to deformation [13–15]. First is the method by which the compressed state of cartilage-on-bone samples is captured and the related structural response analysed using differential interference contrast (DIC) optical microscopy. DIC microscopy enables *fully hydrated* sections to be imaged at levels of resolution where microstructural details of the cartilage matrix deformation may be imaged [13]. DIC, with polarised light microscopy, is able to delineate between structurally different alignments of fibrillar matrix and is able to clearly show boundaries between zones of different fibrillar orientations [13, 14].

Second is the use of a novel compression indenter (see Figure 1 inset) incorporating a central channel relief zone which creates two quite different sites of structural interest, namely, a directly loaded region and an indirectly loaded relief zone which develops within the channel space [14]. This channel-indentation technique, when combined with chemical fixation of the equilibrium deformed state, provides visualisation of the tissue's microstructural response across regions of both direct and nondirect loading. It very effectively captures the subtlety of the microstructural response across the transition between these two regions and offers new insights into both fibrillar interconnectivity and the role of the strain-limiting tangential layer of the cartilage matrix [14–16].

Previous published studies employing the channel indentation technique used only creep loading protocols [14–16]. In this new study, the channel indentation technique was used to compare the depth-dependent structural/deformation response of cartilage-on-bone to compressive loading, comparing the effects of stress relaxation and creep following the application of specific levels of stress. We hypothesize that these different modes of loading will cause differences in matrix deformation at the microlevel and fibrillar level.

2. Materials and Methods

2.1. Cartilage-on-Bone Sample Preparation. Eighteen healthy bovine patellae obtained from prime bulls (≈2-3 years old) were collected immediately following slaughter and stored at −20°C. Each patella was thawed under cold running water and the cartilage surface was stained with India ink to confirm that there were no surface irregularities or fissures [17]. Carefully selecting an optimally flat region, a cartilage-bone block with *en face* dimensions of ~12 mm × 12 mm was sawn from the distal-lateral quadrant of each patella. Each block included the full cartilage thickness and a ~6–10 mm depth of subchondral bone to provide support under load. The block was equilibrated in 0.15 M saline for one hour at 4°C, following which it was then secured with dental cement in a custom-built stainless steel holder, in preparation for mechanical loading.

2.2. Loading Protocol. All loading was performed using a specially designed polished stainless steel indenter consisting of two flat 8×3 mm faces separated by a channel space of 1 mm and channel height of 3 mm. Details of this indenter have been described elsewhere [14]. The loading experiments were conducted using an Instron 5543 materials testing machine with the samples submerged in a 0.15 M saline bath. A stress of either 1 MPa or 7 MPa was applied, following which either the stress was allowed to relax (by holding the indenter position constant) or the stress was maintained to facilitate creep (Figures 1(a) and 1(b)).

For the stress relaxation test protocol, 12 cartilage-on-bone block samples were used. Six samples were ramp loaded at a displacement rate of 10 mm/minute up to 1 MPa and

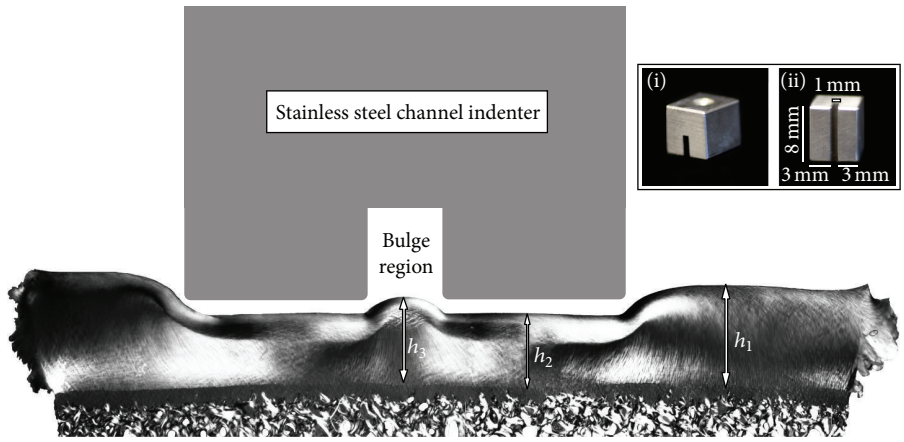

FIGURE 2: An illustration showing the channel indenter (shown in gray) profile in the compressed cartilage tissue. Note the tissue bulge in the channel space (*bulge region*). Microimages from each sample were used to measure h_1: the unloaded thickness, h_2: the directly loaded thickness, and h_3: the bulge height, in order to calculate the normal axial strain and bulge strain. Inset: photo of the steel channel indenter and its dimensions, with the indenter (i) upright and (ii) showing the underside.

then held in position for 2 hours, at which point near-equilibrium stress was achieved as indicated by the force-time curve. Following equilibrium, the saline bath was replaced by 10% formalin and the sample fixed overnight, with the indenter position held and the sample maintained in its deformed state. The other six samples underwent the same process except that they were subject to a ramp load of 7 MPa.

For the creep loading test protocol, 9 cartilage-on-bone block samples were used. Six samples underwent ramp loading at 1 MPa, at 10 mm/minute, following which this stress level was held for 2 hours (until a near-equilibrium creep strain was achieved as determined by the displacement-time graph). Again, following equilibrium, the saline bath was replaced with 10% formalin and the sample fixed overnight in its loaded state. Another three samples underwent the same creep loading procedure but at 7 MPa.

Force, displacement, and time data from the stress relaxation and creep tests, together with the known geometry of the indenter contact area and cartilage thicknesses (see Section 2.3), were used to obtain nominal stresses and strains for each sample tested. From the mechanical data, peak and equilibrium stresses for the stress relaxation experiments, and initial and equilibrium strains for the creep experiments, were obtained (Figure 1).

2.3. Microsection Analysis. Following loading/fixation, each sample was washed in cold running water for 1 hour to remove excess formalin and then mildly decalcified in 10% formic acid solution for 3 days to facilitate sectioning of the osteochondral region [13]. Following the 3 days, the sample was rinsed in cold running water for 1 hour to remove the excess formic acid and halt any further decalcification. A central radial cut was made through each decalcified osteochondral sample to obtain the full cross-sectional profile of the directly and non-directly loaded matrix so as to incorporate the channel region and the wider cartilage continuum. The samples were then quick-frozen and cryosectioned using a sledging microtome to obtain 10–30 μm thick frozen osteochondral sections close to the original radial cut. These sections were then wet-mounted in 0.15 M saline on a glass slide under a cover slip and examined using differential interference contrast (DIC) microscopy.

The tissue thicknesses at different regions were measured from calibrated DIC images (Figure 2). Three different thickness values were measured from a typical microsection, that is, h_1: the unloaded thickness, h_2: the directly loaded thickness, and h_3: the bulge height (see previous descriptions in [14, 16]). Normal axial strain and bulge strain were calculated with the following equations:

$$\text{normal axial strain} = \frac{(h_1 - h_2)}{h_1} \times 100\%,$$
$$\text{bulge strain} = \frac{(h_1 - h_3)}{h_1} \times 100\%. \quad (1)$$

As with our previous cartilage microstructural studies [13, 14], the chondrocytes were utilized as markers to capture the deformation response of the loaded matrix. The overall fibril orientation has been shown to be aligned with the long axis of the chondrocytes [18]. Thus, by mapping the lines of chondrocyte continuity, the generalised fibril orientation within the fields of deformation can be inferred. Although individual fibrils were beyond optical resolution, further confirmation of fibrillar arrangement was still obtainable from the high resolution DIC images. This is because the fibrils, either as a consequence of matrix deformation [13] or degeneration-related destructuring [19, 20], tend to aggregate into larger bundles that give rise to a directional *fibrosity* and thus reflect an overall fibrillar organisation. In order to provide a comparison between the samples loaded in creep versus stress relaxation, their respective patterns of deformation were described in terms of relative changes in profile and orientation of the lines of chondrocyte continuity.

Table 1: Average values obtained from stress relaxation tests. Asterisks indicate significant differences ($p < 0.05$).

Stress relaxation	Peak stress (MPa)	Strain at peak stress (initial strain)	Equilibrium stress (MPa)
Group SR1	1	$0.12 \pm 0.02^*$	$0.09 \pm 0.04^*$
Group SR7	7	$0.31 \pm 0.03^*$	$0.23 \pm 0.10^*$

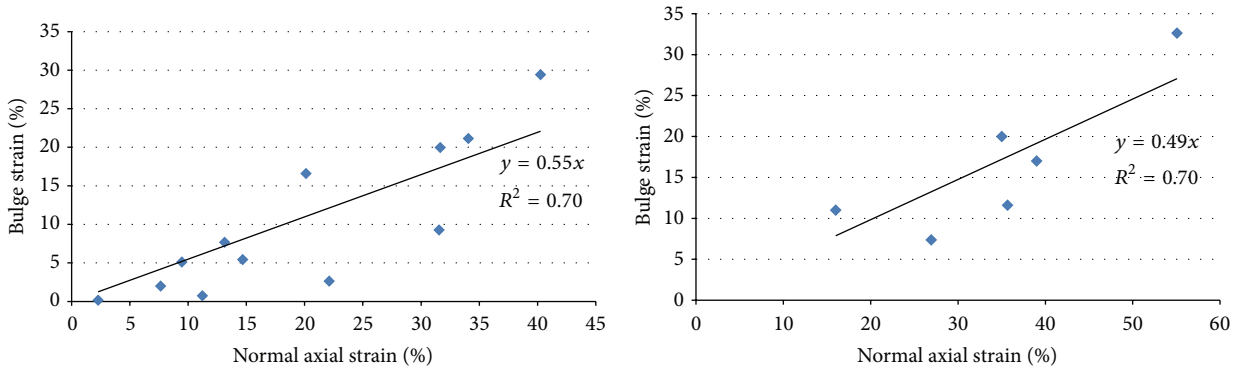

(a) Stress relaxation tests

(b) Creep tests

Figure 3: A plot of the *bulge strain* versus *normal axial strain* for (a) the stress relaxation tests and (b) creep tests, only for Group C1. There is a relatively good correlation between both parameters as indicated by the linear fit.

Table 2: Average values obtained from creep tests.

Creep	Stress (MPa)	Initial strain	Equilibrium strain
Group Cr1	1	0.14 ± 0.03	0.39 ± 0.14
Group Cr7	7	0.37 ± 0.04	0.56 ± 0.08

2.4. Statistical Analysis. The data were organised according to the applied loading protocol, stress relaxation (SR) or creep (Cr), and the amount of loading, 1 MPa (suffix 1) or 7 MPa (suffix 7). This organisation resulted in the following groups: SR1, SR7, Cr1, and Cr7.

Data were presented as means ± standard deviations. Nonparametric analysis Kruskal-Wallis Test, in IBM SPSS Statistics (IBM Corp., Armonk, NY), was employed to check for significant differences ($p < 0.05$). A correlation coefficient was calculated to determine whether there was any significant relationship between any two parameters.

3. Results

3.1. Mechanical Data. Table 1 summarises the mechanical data obtained for groups that underwent *stress relaxation*. In the SR7 samples, compared to the SR1 samples, the initial strain and the equilibrium stress were on average both higher by an equal value of 2.6 times. The stress relaxation ratio (i.e., peak stress to equilibrium stress) for the SR7 group was 2.7 times larger than that in the SR1 group. These differences between SR7 versus SR1 were significant ($p < 0.05$).

Table 2 summarises the mechanical data obtained for groups that underwent *creep* loading. Comparing the Cr7 samples and Cr1 samples, both the initial strain and the equilibrium strain were higher by 2.6 and 1.4 times, respectively. Comparing the initial strains in the stress relaxation and creep samples indicated that within the low and high stress groups there was no significant difference.

3.2. Structural Data. A comparison of cartilage height in the directly loaded and bulge regions (refer to Figure 2) indicated a positive correlation between the bulge strain and the normal axial strains for both the stress relaxation and creep samples (Figure 3).

In the bulge region, microimaging with DIC revealed several consistent differences between and within the stress relaxation and creep groups. "Shear bands," as described in previous creep tests using the channel indenter [14–16], were present in the bulge region of the SR7 and Cr1 samples only (arrows in Figures 4(b) and 4(c)). The shear bands were much less intense in the SR7 group than in the Cr1 group. The Cr7 samples showed microrupture in the bulge region while in the bulge region of the SR1 samples there was no obvious shear band development (Figures 4(b) and 4(c)).

In the directly loaded region, there was a consistent appearance of shear bands in stress relaxation samples from both the SR1 and SR7 groups (Figures 5(a), 5(b), 6, and 7). Conversely, for the creep-loaded samples from the Cr1 group any shear bands that were present were confined to the bulge region (Figures 5(c) and 5(d)). The higher magnification images also show that these shear bands are generated as a consequence of an in-phase compression (crimp) of the fibrillar network (white lines in Figure 6(c)) within a larger scale distortional strain field (white arrows in Figure 6(c)).

In the creep-loaded Cr1 samples, there was a lateral deviation of chondrocyte alignment in the upper midzone to deep matrix of the directly loaded region pointing towards the bulge region (Figure 8). A structural discontinuity (indicated by the dashed arrow in Figure 8) intruded into the bulge region where shear bands were present (region X in Figure 8 and, at higher magnification, in Figures 9 and 10). These bands indicate a relatively abrupt structural discontinuity (boundary between E_1 and E_2 in Figure 9), as depicted by the increasingly acute in-phase compression of the fibrillar

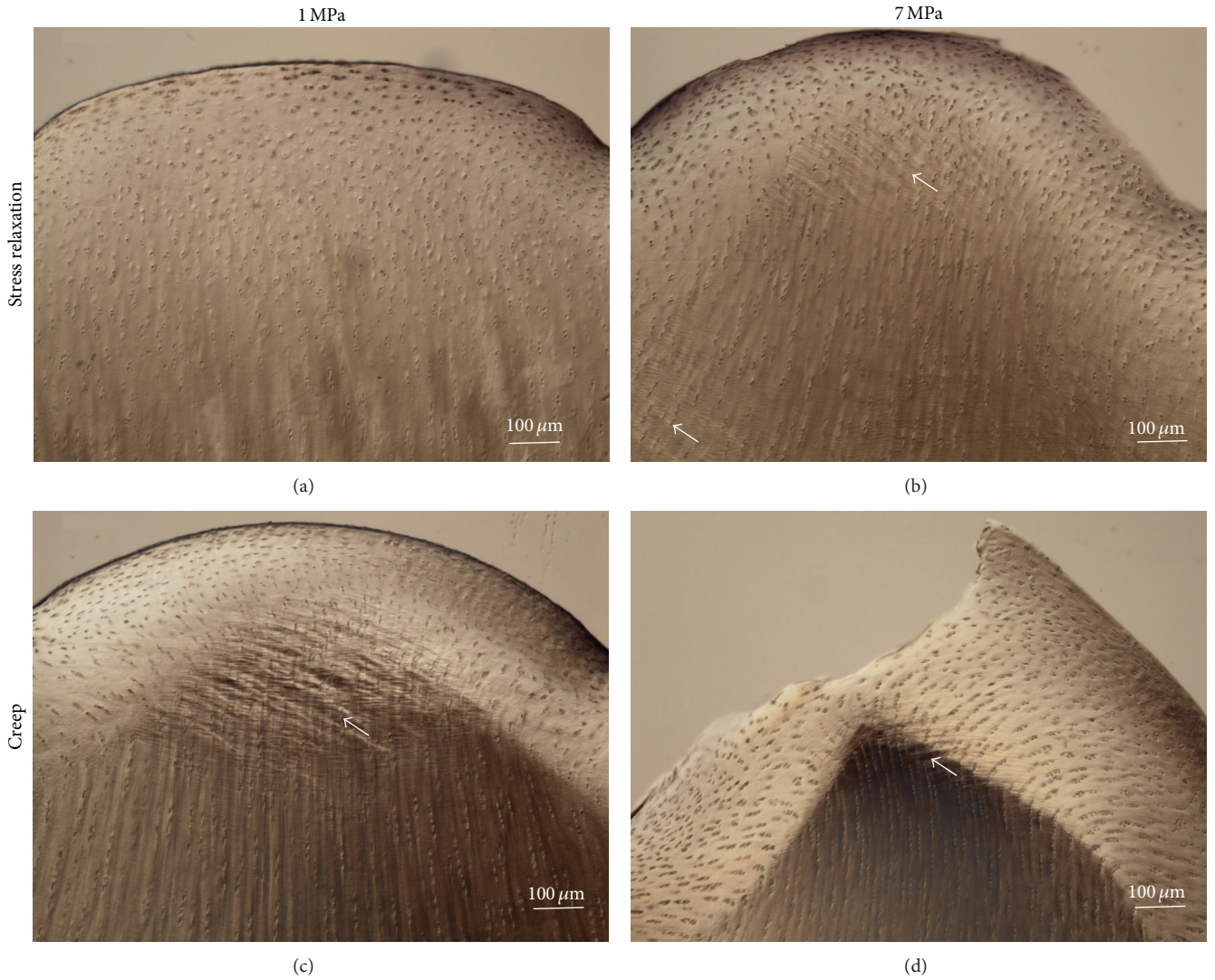

Figure 4: Differential interference contrast (DIC) images of the *bulge region* from typical samples of the four groups studied: (a) SR1, (b) SR7, (c) Cr1, and (d) Cr7, where rupture has occurred. The arrows point to visible shear bands.

matrix (highlighted by the wavy lines in Figure 10). These bands and their lines of force transmission, bending towards the curvature of the bulge, are highlighted by tracing the continuity of the in-phase fibrillar compression (see long arrows in Figure 10).

That the above lines of force transmission are mechanically important is supported by the ruptured bulges in the Cr7 samples. In these high stress ruptures (Figure 11) the shear bands feature was reduced and the lines of force transmission in the remaining upper cartilage layer, while still following the bulge contour, are visible as tension lines (arrows in Figure 11) orthogonal to the fracture path within the matrix (indicated with a "V" in Figure 11).

4. Discussion

This study has allowed for a comparison of the microstructural and mechanical responses of the cartilage-on-bone system under the different loading conditions of stress relaxation and creep. In comparing stress relaxation in Groups SR1 and SR7, the 7-fold difference in the applied stress resulted in the strain at peak stress increasing by only 2.6 times (see Table 1). This effective increase in stiffness is consistent with previous studies showing that the cartilage matrix stiffens with increasing strain [21, 22]. Mansour and Mow [21] attributed this increased stiffening to a *reducing hydraulic permeability* beneath the directly loaded matrix. However, it would be important to note other factors that could also account for the increasing stiffness with the larger strains, such as osmotic pressure increase (negative charges per fluid volume) and an increasingly consolidated solid matrix [23, 24].

The mechanical response to creep was different than to the stress relaxation in that the 7-fold increase in stress resulted in the equilibrium strain increasing by only 1.4 times. Even the 1 MPa (Group Cr1) samples underwent extensive axial strain as the fixed load continued to deform the tissue and contribute to stress development in the bulge region. This

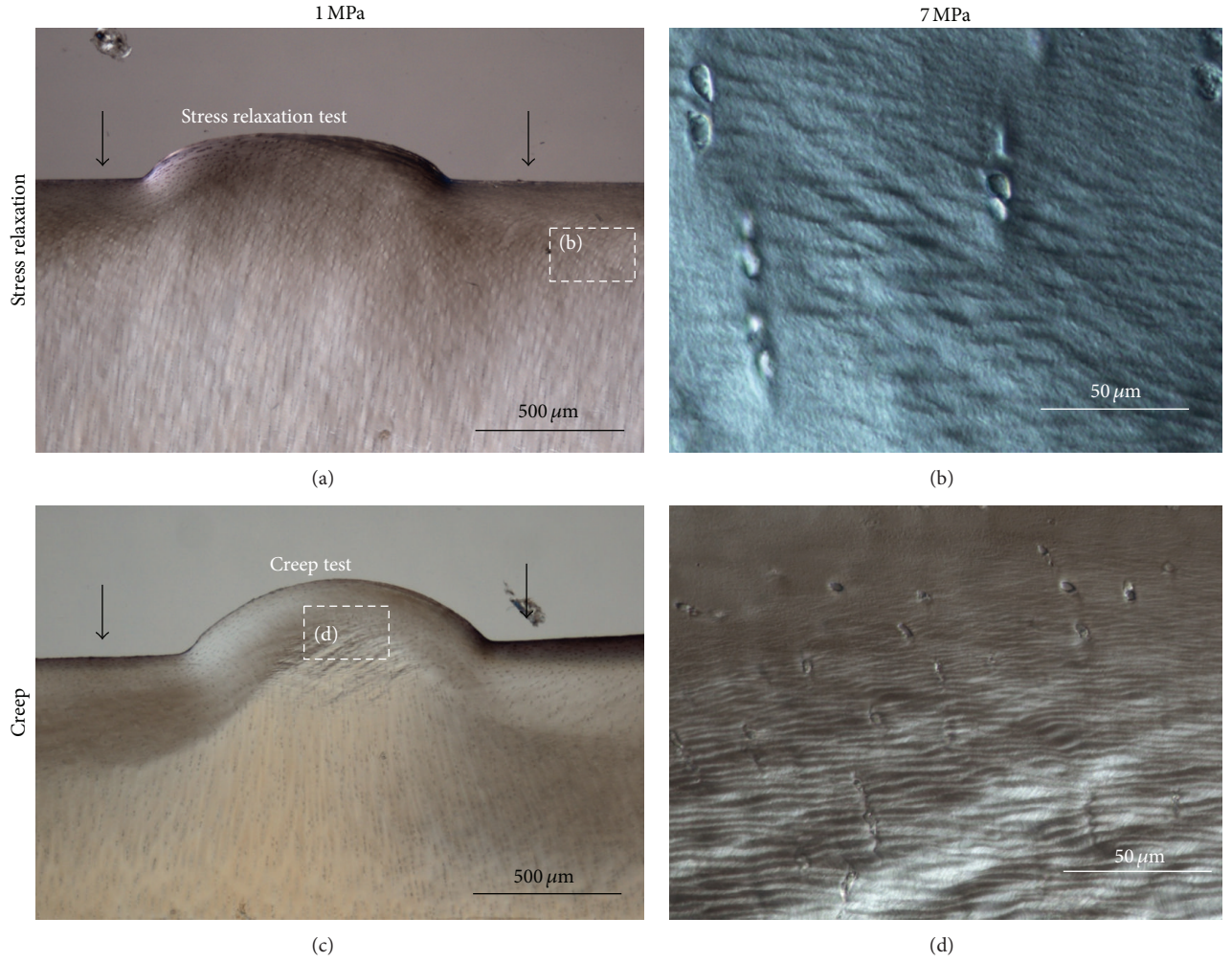

Figure 5: Comparison of the location of shear bands (boxed regions) in samples from (a) SR7 and (c) Cr1. Higher magnification views of the boxed regions are shown in (b) and (d), respectively. DIC imaging.

is evident from the lateral flow in the directly loaded matrix (imaged in Figure 8) and the intense shear band development in the bulge region (Figures 9 and 10). The lateral "bulging" of the tissue in the directly compressed region, when imaged by DIC, showed a clearly visible structural discontinuity (single-head solid arrows in Figure 8) that persisted all the way up to the tissue bulge in the channel region. Further, within the bulge region (refer to Figure 9) there is an obvious material or structural mismatch (demarcated by the dotted line in Figure 9) that can be attributed to known mechanical properties and structural differences within the transition from the tangential surface layer down into the midzone of the cartilage matrix [25–29]. In fact, the region of structural integration of these two strongly differentiated zones (i.e., the surface layer and midzone) which has been described as containing an "arcade" type fibril continuity [30] may have been captured in its functional state in the visible lines of action imaged in the bulge region and transitioning these two zones (Figure 10).

That shear bands formed in the bulge region of the SR7 and Cr1 samples only may be largely attributed to their larger equilibrium strains (30% to 40%) compared to those of the SR1 samples with their lower strains of 12% in which there was an absence of shear bands in the bulge region. It should also be noted that the greater-than-55% equilibrium strains sustained by the Cr7 samples were always accompanied by rupture. This, in turn, would have the effect of relieving the matrix of the very constraints that would have otherwise induced shear band formation. It may also be hypothesized that the shear bands seen in the directly loaded region only in Group SR1 samples are related to the relatively low levels of equilibrium stress in this group (about 0.09 MPa).

Of particular interest is how, in all the Group Cr7 samples, the 7 MPa continuous loading led to the ultimate rupture in the bulge region. Previous studies with the channel indenter have only involved creep loading and reported that at 3.6 MPa the equilibrium strain was 36% [14] and at 4.5 MPa the strain was 56% [15]. In all previous cases rupture of the bulge did not occur. The 56% equilibrium strain measured in Group Cr7 samples (Table 2) was estimated from the ruptured morphology of the bulge and is thus very approximate; however, it does provide a "forensic" insight into the extent to which

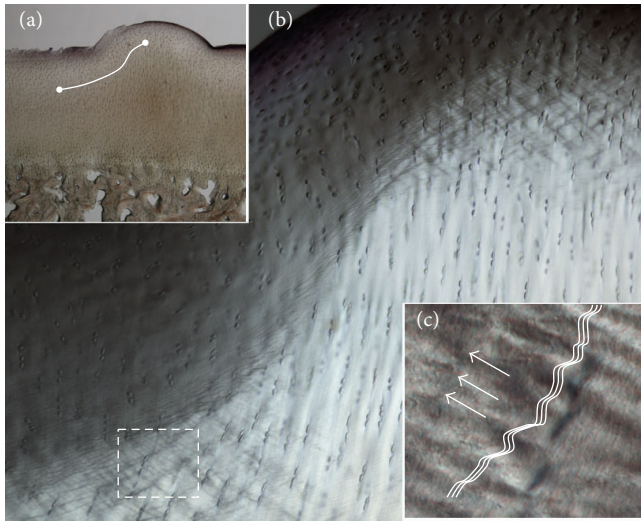

Figure 6: A more detailed view of an SR7 group sample, from the directly loaded region to the bulge region. (a) The white line indicates the span of the region shown at higher magnification in (b). Shear bands are visible as patterns of oblique-crisscross lines. The boxed region (dashed line) in (b) is greatly enlarged in (c) to show the structure of the shear bands. The wave feature represents an in-phase fibrillar compression (crimp) with the arrows indicating the overall direction of this crimp, forming part of the crisscross pattern visible at the larger scale view. DIC imaging.

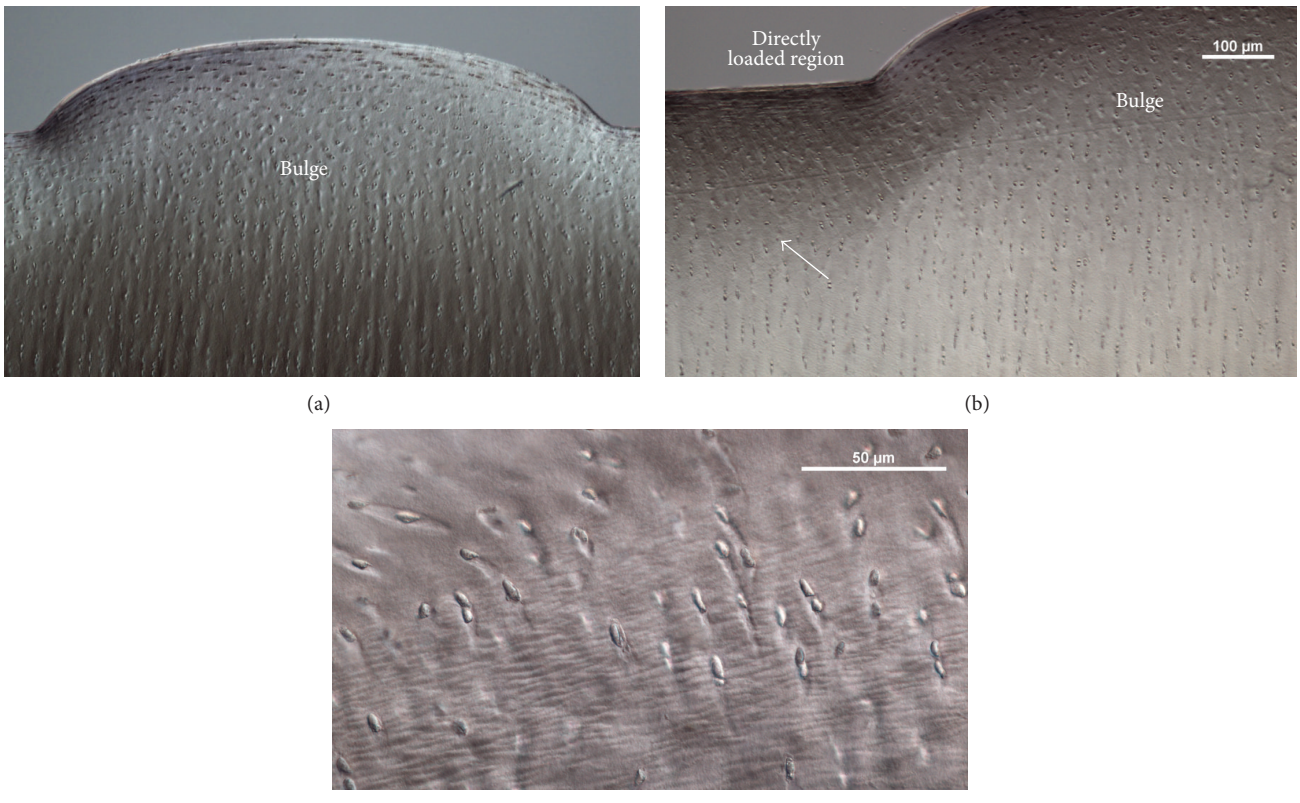

(a) (b)

(c)

Figure 7: Images of a typical sample from the SR1 group. (a) shows the bulge and (b) shows how in a 1 MPa stress relaxation experiment shear bands are present in the directly loaded region (b). The arrow in (b) points to the region shown at higher magnification in (c). DIC imaging.

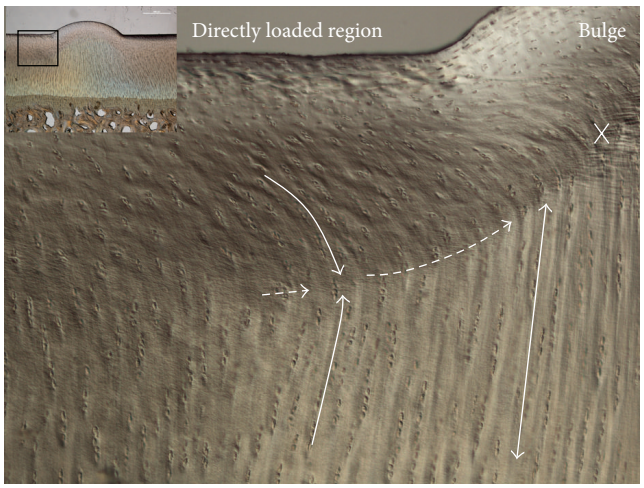

Figure 8: An overview of a Cr1 sample. The main image is a magnification of the boxed region shown in the smaller image. The solid single-headed arrows trace the curvature of chondrocyte alignment and highlight the overall lateral deformation. The dotted arrows indicate a structural discontinuity that persists all the way up to region X, the start of the bulge region, where shear bands form. Region X is imaged at higher magnification in Figures 9 and 10 and discussed accordingly. The double-headed arrow indicates the midzone chondrocyte alignment which appears to be deviated towards the bulge region. DIC imaging.

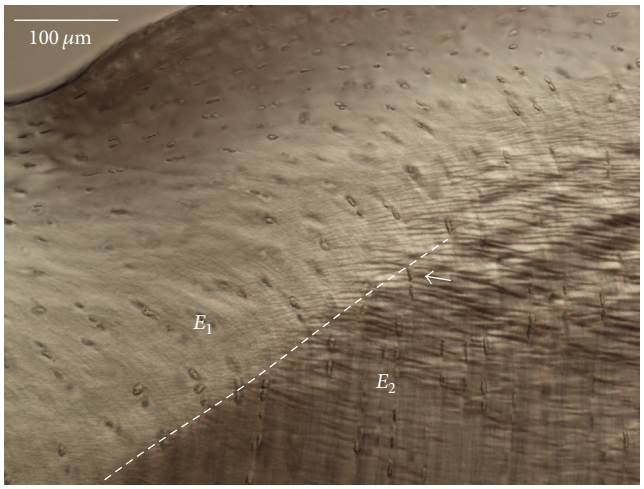

Figure 9: A magnification of region X in Figure 8. The dotted line indicates the structural discontinuity that is obvious between regions E_1 and E_2. The arrow points to the site that was imaged at higher magnification, shown in Figure 10. DIC imaging.

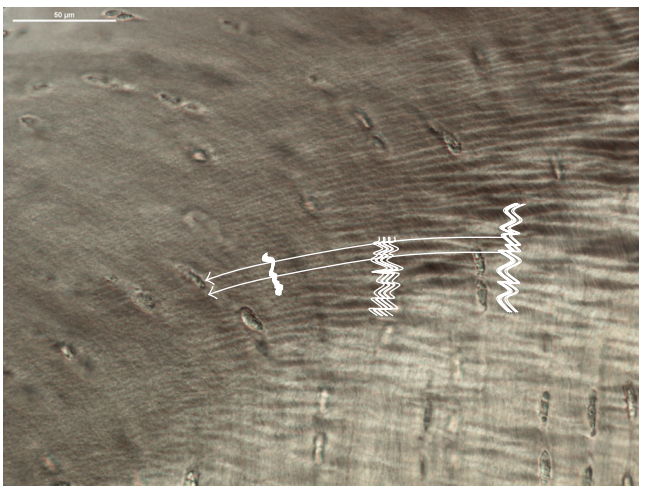

Figure 10: A high magnification image of the region indicated in Figure 9. The wavy lines show the in-phase fibrillar paths. Note the increasingly acute and fine packing moving towards the left. The arrows are drawn by connecting the "peaks and troughs" of the wavy line traces and give an indication of the overall shear direction. DIC imaging.

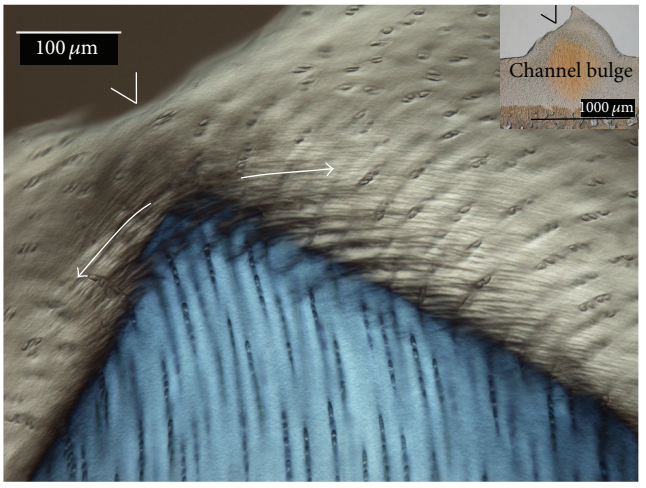

Figure 11: Bulge facture of a Cr7 sample. Following 7 MPa creep loading, samples suffered microfractures in the surface layer of the bulge region, as shown here. The arrows trace the fibrillar in-phase crimping in the surface layer and the "V" indicates the crack path. DIC imaging.

the strain-limiting surface layer may undergo deformation prior to failure. The rupture could therefore be a result of a combination of increasing pressure in the bulge region and a surface layer reaching its strain limit, unable to contain the increasing pressure. This idea is supported by the delineated "lines of action" within the matrix (arrows in Figure 11) transitioning the surface layer to the midzone and orthogonal to the crack direction (see "V" in Figure 11). That the lines of chondrocyte continuity in the mid matrix are all aligned towards the rupture in the surface layer suggests that there is a fluid flow-induced upwards displacement of the matrix in the bulge region which may be implicated in contributing to the rupture. Note also that shear bands are not present in the bulge midzone matrix and this is consistent with a release of stress in this region following surface layer rupture. The tissue bulge from creep loading is assumed to arise from fluid pressure that is being resisted by the strain-limiting surface layer and fibril interconnectivity [14–16].

The structural data from the present study show that when cartilage is consolidated (via creep), the mechanism of force transmission in the solid matrix differs from when

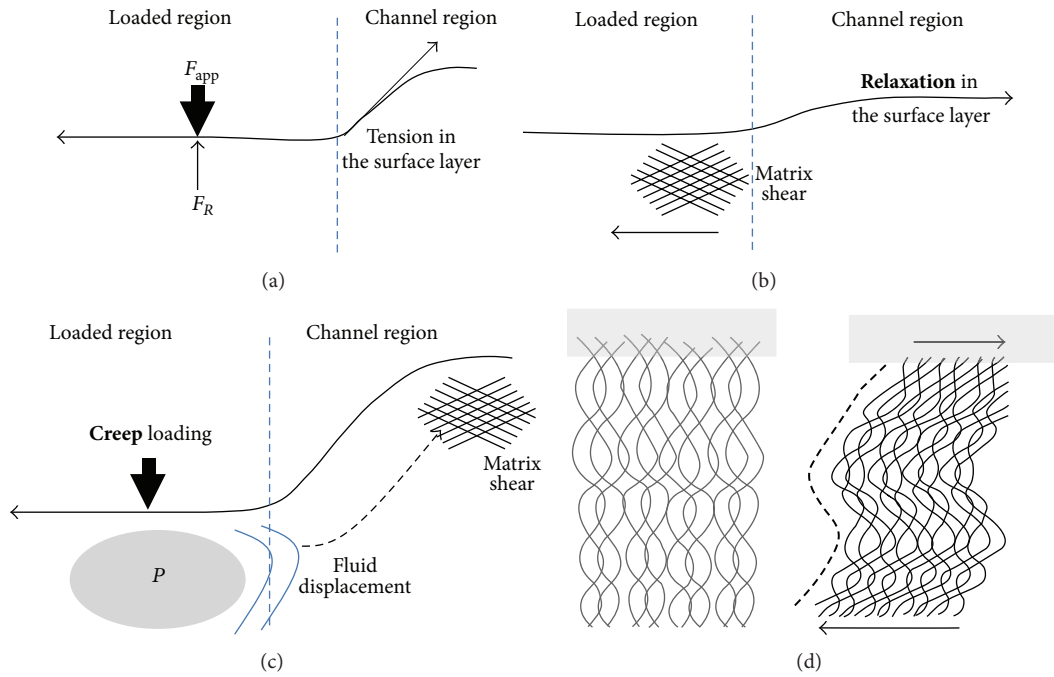

FIGURE 12: (a) Initial compression (F_{app}) of the cartilage tissue creates tension in the surface layer across the directly loaded and non-directly loaded (channel) regions. The matrix reaction is depicted by F_R. (b) With small 1 MPa loads, a smaller compressive strain results, and holding the position following attainment of 1 MPa allows stress relaxation in the surface layer that creates a matrix shear, manifested by the shear bands shown as crisscross pattern. (c) With creep loading of the cartilage tissue, even with small loads, a relatively large compressive strain results from tissue consolidation at this fixed load. Fluid-pressure build-up (P) and fluid displacement into the channel region cause matrix shear (shear bands) to form in the bulge region. (d) Matrix shear or shear bands and how they are formed are illustrated. Shear causes in-phase crimping (indicated with the dotted line) of the interconnected fibrillar matrix that is resolvable at the microscale (refer also to Figures 6(c) and 10).

the stress is allowed to decay as in the stress relaxation experiment. While it is not possible to obtain images of tissue compression at the instant of applying the load, the image data (e.g., Figures 5 and 6), showing variations in the location of the shear bands, provide an indication that there may be different mechanisms at play. At first sight it may appear that the microstructural responses observed in the various groups following the different loading protocols may just be a function of the different resulting strains. However that it is not simply strain that is the influence is supported by our previous investigation on degenerate cartilage showing that, with a range of healthy to severely degenerate samples, creep-loaded to the same axial strain, there were significantly different microstructural responses, between groups, in both the directly loaded and bulge regions [16]. It was found that the role of the microstructural integrity of the strain-limiting tangential layer and the nanolevel interconnectivity of the fibrillar network determined the microstructural to ultrastructural response [16]. In the present study, in applying the loading protocols to study viscoelastic effects, the issue of fluid displacement should also be considered, especially in relation to the different strains and matrix deformation. We thus suggest that the differences in the microstructural response between the stress relaxation and creep loading protocols are due to the interplay of different levels of axial strain in conjunction with the associated fluid pressure that develops in the directly loaded region. In view of such an interplay of strain and fluid pressure, the microstructural responses can be described more specifically in terms of (i) the extent of tension and subsequent relaxation in the surface layer, (ii) the elastic limit of the surface layer, (iii) the fluid pressure build-up in the directly loaded region, and (iv) the interfibrillar connectivity within the zonally differentiated fibrillar architecture.

It is thus proposed that the above four *mechanostructural* mechanisms in cartilage compression be used as primary descriptors of the responses observed in the present study involving stress relaxation versus creep loading. With the application of the 1 MPa load, the underlying matrix and tension in the surface layer support the applied stress (Figure 12(a)). In the stress relaxation samples, the relatively low levels of compressive strain achieved, compared with the creep-loaded samples, result in relatively little fluid pressure build-up beneath the directly loaded region. It is likely that the surface layer in the channel region (non-directly loaded) accommodates most of the stress relaxation by deforming into the bulge observed (Figures 12(b) and 4(a)). With a structural transition between the tangentially aligned fibrillar network in the surface layer and the overall radially aligned underlying matrix, any forces in the surface layer can thus be seen to produce a relative shear with the underlying matrix (Figure 12(b)), the location of which is consistent with the shear band formation in the directly loaded region of the stress relaxation samples (refer to Figure 7).

This *interzonal shear* translates into a matrix distortion due to the transverse connectivity of the fibrillar matrix (Figure 12(d)), resulting in the shear band morphology imaged in the present study (Figure 5(b) and circled region in Figure 6). With creep loading, and increasing compressive strain, the fluid pressure in the directly loaded region builds up ("*P*" in Figure 12(c)), and this is likely to create a positive displacement of fluid towards the relief zone contributing to increasing pressure within the bulge in the channel region. This, in turn, is restrained by the surface layer tension in opposition to the underlying radially aligned fibrillar matrix, resulting in shear band formation (Figures 5(c) and 5(d)).

In summary, therefore, the creep and stress relaxation loading used in the present study resulted primarily in different strain levels, different transient fluid pressure gradients in the tissue, and different patterns of fluid flow over time. In the stress relaxation protocol, with the arrest of any increase in strain and pressure, the initial mode of stress release appears to involve mostly relaxation in the surface layer. In the creep loading protocol, with increasing strain, the main mode of stress release is a lateral distribution of load via the mid matrix and fluid displacement.

5. Conclusions

Two primary modes of stress distribution were observed when cartilage was loaded via stress relaxation or creep, and four *mechanostructural* mechanisms are proposed to account for these differences. These different mechanisms, unique to cartilage structure and function, may serve as important inputs for the biomechanical modelling of this complex tissue.

Conflict of Interests

The authors declare that there is no conflict of interests regarding the publication of this paper.

Acknowledgments

The authors are grateful to the Royal Society of New Zealand and the Marsden Grant Award for funding and supporting this work. Additional support from Arthritis New Zealand is also acknowledged.

References

[1] X. L. Lu and V. C. Mow, "Biomechanics of articular cartilage and determination of material properties," *Medicine and Science in Sports and Exercise*, vol. 40, no. 2, pp. 193–199, 2008.

[2] W. Wilson, C. C. van Donkelaar, R. van Rietbergen, and R. Huiskes, "The role of computational models in the search for the mechanical behavior and damage mechanisms of articular cartilage," *Medical Engineering and Physics*, vol. 27, no. 10, pp. 810–826, 2005.

[3] T. Nguyen and A. Oloyede, "Predictive rheological models for the consolidation behaviour of articular cartilage under static loading," *Proceedings of the Institution of Mechanical Engineers, Part H: Journal of Engineering in Medicine*, vol. 215, no. 6, pp. 565–577, 2001.

[4] V. C. Mow, S. C. Kuei, W. M. Lai, and C. G. Armstrong, "Biphasic creep and stress relaxation of articular cartilage in compression: theory and experiments," *Journal of Biomechanical Engineering*, vol. 102, no. 1, pp. 73–84, 1980.

[5] V. C. Mow, M. H. Holmes, and W. M. Lai, "Fluid transport and mechanical properties of articular cartilage: a review," *Journal of Biomechanics*, vol. 17, no. 5, pp. 377–394, 1984.

[6] A. Oloyede, R. Flachsmann, and N. D. Broom, "The dramatic influence of loading velocity on the compressive response of articular cartilage," *Connective Tissue Research*, vol. 27, no. 4, pp. 211–224, 1992.

[7] C.-Y. Huang, M. A. Soltz, M. Kopacz, V. C. Mow, and G. A. Ateshian, "Experimental verification of the roles of intrinsic matrix viscoelasticity and tension-compression nonlinearity in the biphasic response of cartilage," *Journal of Biomechanical Engineering*, vol. 125, no. 1, pp. 84–93, 2003.

[8] C.-Y. Huang, V. C. Mow, and G. A. Ateshian, "The role of flow-independent viscoelasticity in the biphasic tensile and compressive responses of articular cartilage," *Journal of Biomechanical Engineering*, vol. 123, no. 5, pp. 410–417, 2001.

[9] R. K. June, S. Ly, and D. P. Fyhrie, "Cartilage stress-relaxation proceeds slower at higher compressive strains," *Archives of Biochemistry and Biophysics*, vol. 483, no. 1, pp. 75–80, 2009.

[10] R. M. Schinagl, D. Gurskis, A. C. Chen, and R. L. Sah, "Depth-dependent confined compression modulus of full-thickness bovine articular cartilage," *Journal of Orthopaedic Research*, vol. 15, no. 4, pp. 499–506, 1997.

[11] W. Wilson, J. M. Huyghe, and C. C. van Donkelaar, "Depth-dependent compressive equilibrium properties of articular cartilage explained by its composition," *Biomechanics and Modeling in Mechanobiology*, vol. 6, no. 1-2, pp. 43–53, 2007.

[12] M. C. van Turnhout, S. Kranenbarg, and J. L. van Leeuwen, "Contribution of postnatal collagen reorientation to depth-dependent mechanical properties of articular cartilage," *Biomechanics and Modeling in Mechanobiology*, vol. 10, no. 2, pp. 269–279, 2011.

[13] A. Thambyah and N. Broom, "Micro-anatomical response of cartilage-on-bone to compression: mechanisms of deformation within and beyond the directly loaded matrix," *Journal of Anatomy*, vol. 209, no. 5, pp. 611–622, 2006.

[14] A. Thambyah, L. Zhao, and N. Broom, "Microstructural response and fluid flow mechanisms in cartilage loading: new insights using a novel indentation method," *Journal of Strain Analysis for Engineering Design*, vol. 44, no. 5, pp. 319–326, 2009.

[15] S. L. Bevill, A. Thambyah, and N. D. Broom, "New insights into the role of the superficial tangential zone in influencing the microstructural response of articular cartilage to compression," *Osteoarthritis and Cartilage*, vol. 18, no. 10, pp. 1310–1318, 2010.

[16] A. Thambyah, J.-Y. Zhao, S. L. Bevill, and N. D. Broom, "Macro-, micro- and ultrastructural investigation of how degeneration influences the response of cartilage to loading," *Journal of the Mechanical Behavior of Biomedical Materials*, vol. 5, no. 1, pp. 206–215, 2012.

[17] G. Meachim, "Light microscopy of Indian ink preparations of fibrillated cartilage," *Annals of the Rheumatic Diseases*, vol. 31, no. 6, pp. 457–464, 1972.

[18] M. J. Kääb, K. Ito, B. Rahn, J. M. Clark, and H. P. Nötzli, "Effect of mechanical load on articular cartilage collagen structure: a scanning electron-microscopic study," *Cells Tissues Organs*, vol. 167, no. 2-3, pp. 106–120, 2000.

[19] M.-H. Chen and N. Broom, "On the ultrastructure of softened cartilage: a possible model for structural transformation," *Journal of Anatomy*, vol. 192, no. 3, pp. 329–341, 1998.

[20] M.-H. Chen and N. D. Broom, "Concerning the ultrastructural origin of large-scale swelling in articular cartilage," *Journal of Anatomy*, vol. 194, no. 3, pp. 445–461, 1999.

[21] J. M. Mansour and V. C. Mow, "The permeability of articular cartilage under compressive strain and at high pressures," *The Journal of Bone and Joint Surgery—American Volume*, vol. 58, no. 4, pp. 509–516, 1976.

[22] E. Langelier and M. D. Buschmann, "Increasing strain and strain rate strengthen transient stiffness but weaken the response to subsequent compression for articular cartilage in unconfined compression," *Journal of Biomechanics*, vol. 36, no. 6, pp. 853–859, 2003.

[23] S. Hosseini, Y. Wu, K. Ito, and C. C. van Donkelaar, "Mechanical evaluation of the mechanism of load transfer in articular cartilage," *Orthopaedic Research Society Transactions*, vol. 36, article 1173, 2012.

[24] A. Oloyede and N. D. Broom, "The generalized consolidation of articular cartilage: an investigation of its near-physiological response to static load," *Connective Tissue Research*, vol. 31, no. 1, pp. 75–86, 1994.

[25] A. Verteramo and B. B. Seedhom, "Zonal and directional variations in tensile properties of bovine articular cartilage with special reference to strain rate variation," *Biorheology*, vol. 41, no. 3-4, pp. 203–213, 2004.

[26] A. Changoor, M. Nelea, S. Méthot et al., "Structural characteristics of the collagen network in human normal, degraded and repair articular cartilages observed in polarized light and scanning electron microscopies," *Osteoarthritis and Cartilage*, vol. 19, no. 12, pp. 1458–1468, 2011.

[27] C. Glaser and R. Putz, "Functional anatomy of articular cartilage under compressive loading quantitative aspects of global, local and zonal reactions of the collagenous network with respect to the surface integrity," *Osteoarthritis and Cartilage*, vol. 10, no. 2, pp. 83–99, 2002.

[28] H. Hedlung, S. Mengarelli-Widholm, F. P. Reinholt, and O. Svensson, "Stereologic studies on collagen in bovine articular cartilage," *APMIS*, vol. 101, no. 2, pp. 133–140, 1993.

[29] N. D. Broom and D. L. Marra, "Ultrastructural evidence for fibril-to-fibril associations in articular cartilage and their functional implication," *Journal of Anatomy*, vol. 146, pp. 185–200, 1986.

[30] A. Benninghoff, "Form und bau der gelenkknorpel in ihren beziehungen zur function," *Zeitschrift fur Zellforschung*, vol. 2, pp. 783–862, 1925.